# Structures induced by small moonlets in Saturn's rings: Implications for Cassini Mission

M. Seiß[1] , H. Salo[2] , M. Sremčević[1] and F. Spahn[1]

M. Seiß, Department of Physics, Nonlinear Dynamics, University of Potsdam, Am Neuen Palais 10, Haus 19, 14469 Potsdam, Germany. (martins@agnld.uni-potsdam.de)

H. Salo, Department of Physical Science, Astronomy Division, University of Oulu, PO Box 3000, FIN-90014 Oulun yliopisto, Finland. (heikki.salo@oulu.fi)

M. Sremčević, Department of Physics, Nonlinear Dynamics, University of Potsdam, Am Neuen Palais 10, Haus 19, 14469 Potsdam, Germany. (msremac@agnld.uni-potsdam.de)

F. Spahn, Department of Physics, Nonlinear Dynamics, University of Potsdam, Am Neuen Palais 10, Haus 19, 14469 Potsdam, Germany. (frank@agnld.uni-potsdam.de)

[1]Department of Physics, Nonlinear Dynamics, University of Potsdam, Potsdam, Germany.

[2]Department of Physical Science, Astronomy Division, University of Oulu, Finland.

Particle simulations are applied to predict density features caused by small moonlets embedded in a dense planetary ring. For the first time a generation of a "propeller" are found together with adjacent density wakes. Both features are clear indications for the existence of moonlets in the rings. The propeller scales with the Hill-radius in radial direction whereas its azimuthal extent is determined by the ratio between the moonlet-mass and the ring-viscosity. Our findings bear direct implications for the analysis of the Cassini-imaging data: (i) for the detection of embedded larger bodies in Saturn's rings, and (ii) for remotely probing transport properties of the rings. The existence of a moonlet-family may point to a catastrophic disruption of a parent body as a formation scenario for rings.

## 1. Introduction

Saturn's dense rings consist of icy particles ranging in size from a few centimeters up to several meters. Furthermore, some bigger bodies are also expected to exist in the rings with sizes of tens of meters up to kilometers. It is known that the gravity of moonlets produce wave-like structures (wakes) (*Cuzzi and Scargle* [1985]; *Showalter et al.* [1986]; *Lewis and Stewart* [2000]), gaps with a ringlet around the moonlet orbit (*Henon* [1981]; *Lissauer et al.* [1981]; *Spahn and Wiebicke* [1989]; *Spahn and Sponholz* [1989]; *Hanninen* [1993]) and S-shaped density structures (propellers) (*Spahn and Sremčević* [2000]; *Sremčević et al.* [2002]). Theories about gaps and wakes combined with the analysis of the Voyager data predicted a few satellites in Saturn's rings (*Lissauer et al.* [1981]; *Showalter et al.* [1986]; *Spahn and Sponholz* [1989]). So far, the investigations have yielded the discovery of only a single satellite (Pan) in the Encke division (*Showalter* [1991]).

The probabilistic scattering model by *Spahn and Wiebicke* [1989] is designed for larger moonlets (diameter: $D \geq 1$ km) where the diffusion scales are negligible compared to the Hill radius

$$h = a_0 \left( \frac{M_\mathrm{m}}{3M_\mathrm{s}} \right)^{1/3} \tag{1}$$

measuring the gravitational range of the moon. The masses of the moonlet and Saturn as well as the semi-major axis of the moonlet are denoted by $M_\mathrm{m}$, $M_\mathrm{s}$ and $a_0$, respectively. It has been shown that the radial extent of the formed gap scales with the Hill radius h. The impact parameter $b = (r - a_0)/h = x/h$ denotes the scaled radial distance from the moonlet, whereas x is the radial coordinate in physical units. It was found that (a) a ringlet is formed at $|b| \leq 1.5$, (b) gaps flank the ringlet at $1.5 \leq |b| \leq 4$ with the radial minima at $|b_\mathrm{min}| = 2$ and (c) wakes appear in

the outer regions $|b| \geq 4$. For even larger moons ($D \geq 3$ km) the gap width scales with $h^2$ (*Petit and Henon* [1988]).

However, this model is inappropriate for smaller moonlets with a much weaker gravity, in which case viscous diffusion of particles becomes important. It counteracts the tendency of the moonlet to create a gap. Therefore *Spahn and Sremčević* [2000] and *Sremčević et al.* [2002] extended the theory of gravitational scattering, by adding nonlinear diffusion of the ring material. They described the diffusion using a hydrodynamical model based on the mass- and momentum balances. Solutions of the related balance equations revealed a scaling of the diffusion equation in azimuthal direction as

$$K = \frac{\Omega_0 h^3}{2(1+\beta)\nu_0 a_0}, \tag{2}$$

giving the scaled azimuthal coordinate $\phi = y/(a_0 K)$, whereas y is the azimuthal distance from the moonlet. The Keplerian frequency is $\Omega_0 = \sqrt{GM_\mathrm{s}/a_0^3}$. The scaling parameter K is determined by the ratio $h^3/\nu_0 \propto M_\mathrm{m}/\nu_0$, where the ring kinematic viscosity is denoted by $\nu_0$. Knowing $M_\mathrm{m}$ from the radial features of the propeller, which scale with $h$, an analysis of the azimuthal structures allow to an estimate of the viscosity $\nu_0$. The coefficient $\beta = \partial \ln \nu / \partial \ln \tau \approx 1$ arises from the assumption $\nu = \nu_0 \cdot (\tau/\tau_0)^\beta$ (*Schmit and Tscharnuter* [1995]; *Salo et al.* [2001]), where $\tau$ is the optical depth of the ring. In spite of the improvement of the scattering model due to the consideration of dissipative processes, a couple of restrictive assumptions have been necessary for its derivation. The most important ones are (i) the reduction of the scattering region to a line, (ii) the neglect of collisions during the scattering and (iii) the azimuthal velocity component is taken to be the Keplerian circular velocity $u_\phi = \sqrt{GM_\mathrm{s}/r}$. In order to check the influence of these simplifications and to verify the predictions (*Sremčević et al.* [2002]), we

carry out local numerical N-body simulations. This alternative approach addionally offers the possibility to investigate the influence of the moonlet induced wakes on the propeller as well as to resolve the density structures in the scattering region. Here, we focus mainly on a verification of the scalings of the propeller extent, predicted by the theory (*Spahn and Sremčević* [2000]).

## 2. Method

For the N-body particle simulations we use the local box method, first introduced for rings by *Wisdom and Tremaine* [1988] and further elaborated by *Salo* [1991, 1995]. The box, with half-widths $L_x$ and $L_y$ in radial and azimuthal directions, is filled with N particles, representing a dynamical optical depth

$$\tau = \frac{\pi N R^2}{4 L_x L_y}. \tag{3}$$

Test simulations suggest $L_x = 9h$ and $L_y$ = 2.8 $K \cdot a_0$ to be the optimum size of the calculation region - large enough to cover the main structures and still manageable numerically. In our simulations we fixed $\tau$ to 0.08, requiring N = 2,900 ... 190,000 particles for moonlets of a radius $R_\mathrm{m}$ = 7 ... 20 meters. It must be noted the upper size is just limited by the current computer performance, but nevertheless the reliability of the scalings becomes better for larger moonlets. Therefore the applicability of the here proved scalings are valid for a bigger class of moonlets with radii up to approximately 500 m. The particles in the calculation region are modeled by inelastic hard spheres with a radius $R$ = 1 m. We simulated a situation in the B-ring of Saturn, i.e. $a_0$ = $10^{-8}$ m corresponding to $h = 1.35 R_\mathrm{m}$ for an icy moonlet ($\rho$ = 900 kg $\mathrm{m}^{-3}$). However, the results can also be scaled to other planetocentric distances provided that $h/R_\mathrm{m} \propto a_0 \rho^{-1/3}$ is fixed. A constant coefficient of restitution $\epsilon$ = 0.5 has been chosen for the collisions. Apart from the inelastic collisions, the motion of the particles around the moonlet

is described by the Hill equations (e.g. *Salo* [1991]). The moonlet is placed in the center of the box. In horizontal direction gravitational interactions between the particles are not included whereas in vertical direction the self gravity is approximated solely via an enhanced vertical frequency $\Omega_z = 3.6 \cdot \Omega_0$ (*Wisdom and Tremaine* [1988]; *Salo* [1991]). Thus the simulations can not model spontaneous gravitational wakes produced by the gravity of the small ring particles (*Salo* [1992, 1995]). However the moonlet ($R_{\rm m} > 100$) induced structures should be much larger than the gravity-wakes, i.e. corresponding to moonlets structures, which could be observed by the Cassini cameras.

Usually periodic boundary conditions are used in the radial as well as in the azimuthal direction (*Wisdom and Tremaine* [1988]; *Salo* [1991, 1995]). Because we are not able to simulate the whole azimuthal extent of the propeller, the particles are still perturbed by the moonlet when they leave the calculation region downstream of the moonlet. Therefore the incoming flux of particles would not correspond to an unperturbed ring flow if periodic boundaries were used. To avoid this, we drop the azimuthal periodic boundary conditions and utilize separate simulations without a moonlet, but with periodic boundary conditions to sample the unperturbed velocity distribution. Then, we use this data (particles' position and velocity while crossing the boundary) to simulate the incoming flow of the perturbed simulation cell at the azimuthal boundaries (see Figure 1). In the radial direction we keep the periodic boundary conditions.

## 3. Results

Figures 2(a) - 2(c) show the optical depth $\tau$ for simulations with different moonlets (moon radius: $R_{\rm m}$ = 7, 12, 20 m). The gray-coded density plots have been calculated by averaging a series of snapshots of the system, after the structures have reached stationarity (typically 10

snapshots per orbital period and altogether 25 orbital periods for the largest moonlet and 500 for the smallest one). This approach reduces considerably the fluctuations of the densities.

All figures show a S-shaped structure, where the moonlet tries to generate a gap whereas collisional diffusion replenishes the material along increasing azimuthal distance $\phi = y/(a_0 \cdot K)$. Density wakes are evolve adjacent to the propeller gaps ($|b| \geq 2$). The phase of the wakes does not scale with $K$, but rather with azimuthal wave number $|\tilde{m}| = 2a_0/(3hb)$ (*Showalter et al.* [1986]), reading in our notation

$$|m| = \frac{\Omega_0 \cdot h^2}{3(1+\beta)\nu_0} \cdot \frac{1}{b}. \tag{4}$$

That means the wake azimuthal spacing $\Delta\phi = 2\pi/m$ is proportional to $M_{\mathrm{m}}^{-2/3}$, if the azimuthal direction is scaled with $K$. This explains the increasing number of wake trains with increasing moonlet sizes.

Figure 2(d) shows the propeller of a $R_{\mathrm{m}}$ = 17 m sized moonlet as it might be seen by the Cassini cameras. The extension of the propeller is much larger in azimuthal direction than in the radial one. The moonlet location is marked by the kink in the gap at $\phi = b = 0$.

In order to check the scalings of the propeller, in figure 3 the radial and azimuthal profiles corresponding to different moonlets have been plotted using scaled units for comparison. All radial profiles have been averaged over the azimuth in order to cancel wake effects. Furthermore we excluded the region where the moonlet gravity dominates the structure ($\phi = y/(a_0 \cdot K) < 1$), because we do not expect that the scalings are applicable there. Figure 3(a) shows a surprisingly good agreement between the radial profiles for all different moonlets. Small differences are well explained by the noise in the profile arising from the finite number of particles in the box. The minimum of the gap is located at $|b| = 2$ in all cases, like in the simulations without diffusion

(*Spahn and Wiebicke* [1989]). This indicates that the collisions occurring in the Hill region close to the moonlet change the character of the scattering only slightly.

In figure 3(b) the azimuthal profiles are presented for a cut at $|b| = 2$, where the minimum of the gap is located. Beyond a critical value $\phi > \phi_{\rm c}(M_{\rm m})$, which marks the region of gravitational influence of the moonlet, all profiles converge to almost a single line. A good agreement is found with the theoretical prediction by *Spahn and Sremčević* [2000] and *Sremčević et al.* [2002] indicating that the azimuthal extent scales with $K$. We also fitted the analytical solution (*Sremčević et al.* [2002], equation presented in figure 10 (c)), in the numerical results, which provides an estimate of the azimuthal scale $K$ = 0.14 m$^{-2} \cdot h^3/a_0 = 0.9 \cdot 10^{-4}$ m kg$^{-1} M_{\rm m}/a_0$. This value K corresponds to an kinematic shear viscosity $\nu_{0,\rm p}$ = 3 cm$^2$ s$^{-1}$ in the perturbed region, provided that $\beta \approx 1$ is used. In the unperturbed calculation cell we measured a viscosity of $\nu_{0,\rm u}$ = 1.2 cm$^2$ s$^{-1}$. Both measured viscosities are of the same order of magnitude, delivering a fair agreement between simulations and theory. The difference between the two values $\nu_0$ can be explained due to the simplifying assumptions made in the analytical model. The perturbed optical depth varies between $\tau/\tau_0 = 0.2...1.3$ meaning that the deviations of the mean optical depth $\tau_0$ are not small as assumed (*Sremčević et al.* [2002]). Because of this considerable variations the the coefficient $\beta$ is not expected to be constant (*Salo et al.* [2001]).

The symbols in the plot 3(b) represent simulations with $R_{\rm m}$ = 10 m, but using different azimuthal box sizes ($L_y$ = 1 ... 5.4 $K \cdot a_0$). The results agree quite well, demonstrating the independence of our results with respect to the box size. The small inserted plot represents a cut at $|b|$ = 1.5. At this radial position the density depletion is still noticeable, and most importantly,

the wakes do not influence the profile. Here the convergence of the lines for growing azimuthal length is even more impressive.

At smaller azimuthal longitudes the scaling does not work anymore because of the finite size of the scattering region and the stronger dominance of the wakes in the gap. The critical value $\phi_{\rm c}(M_{\rm m})$ shrinks with increasing moonlet mass, indicating that the concept of a scattering line mimicking the Hill sphere becomes more and more realistic the bigger the moonlets are (see also figures 2(a) - 2(c)).

Figures 4(a) - 4(c) show a zoomed part of the region of interest whereas the analytical solution (*Sremčević et al.* [2002]) is plotted in figure 4(d) for comparison. The wakes are still prominent in the region of the gap up to $|b_{\rm wakes}| \geq 2$ in contrast to the wake model (*Showalter et al.* [1986]) where wakes occur at $|b_{\rm wakes}| \geq 4$. Of course, the wakes cannot be described with the scattering model (*Spahn and Sremčević* [2000]; *Sremčević et al.* [2002]), because azimuthal structures are averaged out, except for the gap. However, our numerical experiments take into account all those effects leading to a propeller interfering density wakes – a pattern which can be expected to show up in Saturn's rings provided larger bodies ($R_{\rm m} > 20$ m) are embedded. In all cases, the maximal extent in azimuthal direction of the contour lines agree fairly well with each other, confirming the scaling predicted by theory. This is even more astonishing having in mind that the azimuthal length of the figures represent 340 m for the $R_{\rm m}$= 7 m moonlet in contrast to 8000 m for the $R_{\rm m}$ = 20 m moonlet.

## 4. Discussion

Simulations with embedded moons have been run for moonlets with different sizes $R_{\rm m}$ = 7 ... 20 m. Larger moonlets as well as self gravity could not be included because of the limiting

computer performance. On the other hand the analytical model is based on assumptions to work well for moonlets larger than 100 m, and in that view our current results are very encouraging. The scalings seem to be valid for about an order of magnitude smaller moonlets, which are in any case expected to be more abundant than the much larger ones. Further it has been shown that the moonlet induced wakes do not influence noticeable the scaling laws of the propeller. The model (*Sremčević et al.* [2002]) predicts that the threshold moonlet size separating propeller structures and gaps is around 500 m ($\nu_0 = 10$ cm$^2$ s$^{-1}$), depending on the ring viscosity. Larger moonlets are able to sweep free a complete gap. Circumference extended structures are certainly easier to detect, but probably harder to associate with moonlets. Self gravity wakes are characterized by the critical wavelength $\lambda_{\rm cr} \approx 100$ m and the pitch angle $\alpha = 20°...25°$. The gap width of the propeller is approximately 2.5h and becomes larger than $\lambda_{\rm cr}$ for $R_{\rm m}$ = 30 m. For $R_{\rm m} > 100$ m the characteristic length scales of the propeller $L_r = 10h \approx 1.3$ km and $L_\phi = 2 \cdot 50 K a_0 \approx 4 \cdot 10^4$ km ($\nu_0 = 3$ m$^2$ s$^{-1}$, $\beta = 1$; cp. *Sremčević et al.* [2002]) are much larger than $\lambda_{\rm cr}$. The pitch angle of the gravity-wakes can be compared with the ratio of the propeller extensions $\tan\alpha = L_{\rm r}/L_\phi \propto h^{-2}$, meaning moonlets with $R_{\rm m} = 0.5...5$ m ($\nu_0 = 1...100$ cm$^2$ s$^{-1}$, $\beta$ = 1) would have a comparable tilt like the gravity wakes. However we are interested in propellers of larger moonlets which are azimuthal elongated structures in contrast to the tilted wakes. Summarizing, selfgravity wakes could superimpose the propeller-wake structure on small length scales. Further the modified viscosity (*Daisaka et al.* [2001]) might increase the efficiency of the radial transports. Therefore also large moonlets (> 500m) could create propellers and not gaps going around the whole circumference. However the propellers and wakes caused by moonlets $R_{\rm m} > 30$ m cannot be destroyed by the selfgravity.

On July 1, 2004 Cassini arrived at Saturn and started delivering data of much higher resolution than ever collected from a space probe at Saturn before. This offers a great chance to discover moonlets (200 m ... 500 m) embedded in the rings, by applying the results of our scattering model - especially scalings confirmed here - to the ISS-imaging- and the UVIS-occultation data of the Cassini spacecraft. In this context the characteristic shape of the kink determined here would reveal the location of the moonlet in the images of the narrow angle camera. There the radial location of the gap minimum changes suddenly from about -2h to +2h, which corresponds to roughly 1000 m for a moonlet of $R_{\rm m}$ = 200 m and to about 2500 m for a moonlet with $R_{\rm m}$ = 500 m. For comparison, the published imaging data of Cassini at Saturn orbit insertion (SOI) had their highest spatial resolution of about 300 m.

Now the probability shall be roughly estimated to detect a moonlet in a Cassini image. The particle size distribution can be modeled by a two sided power law $n(R) \propto R^{-q}$ assuming e.g. the ring has been formed by a catastrophic disruption of a parent body. *French and Nicholson* [2000] estimated from stellar occultation observations of the outer A-ring $q$ = 2.9 for particles $R$ = 1 cm ... 20 m. Hence a sharp knee is expected for larger particles $R > 20$ m with a steeper distribution. Provided that the moonlet Pan is the largest fragment of the disruption a power law with $q$ = 6 would be plausible for particles $R > 20$ m. Density structures of moonlets $R_{\rm m}$ = 200 m ... 500 m can be discovered in the high resolution SOI images. The detection probability of this size class can be estimated to 4 particles per image.Similar results can be predicted with parameter of the inner A and the B ring, promising a good chance to find a moonlet. Once a moonlet has been found imaging (ISS) and additionally high resolution occultation (UVIS,RSS) data could help to analyse the propeller shape and to deduce the mass of the moonlet as well as

the viscosity of the ring material from the scalings laws. Finally if enough moonlets are found, it becomes possible to gain information about distributions (size, position etc.) of such bodies, containing hints about the origin of Saturn's rings.

**Acknowledgments.** We thank Jürgen Schmidt for many useful discussions. This work was supported by the Deutsche Forschungsgemeinschaft (DFG), Deutsches Zentrum für Luft- und Raumfahrt (DLR), Väisälä Foundation and the Academy of Finland.

## References

Cuzzi, J. N., and J. D. Scargle (1985), Wavy edges suggest moonlet in Encke's gap, *Astrophys. J.,* , *292*, 276–290.

Daisaka, H., H. Tanaka, and S. Ida (2001), Viscosity in a Dense Planetary Ring with Self-Gravitating Particles, *Icarus*, *154*, 296–312.

French, R. G., and P. D. Nicholson (2000), Saturn's Rings II. Particle sizes inferred from stellar occultation data, *Icarus*, *145*, 502–523.

Greenberg, R., and A. Brahic (Eds.) (1984), *Planetary rings*, The University of Arizona Press.

Hanninen, J. (1993), Numerical simulations of moon-ringlet interaction, *Icarus*, *103*, 104–123.

Henon, M. (1981), A simple model of Saturn's rings, *Nature* , *293*, 33–35.

Lewis, M. C., and G. R. Stewart (2000), Collisional Dynamics of Perturbed Planetary Rings. I., *Astron. J.,* , *120*, 3295–3310.

Lissauer, J. J., F. H. Shu, and J. N. Cuzzi (1981), Moonlets in Saturn's rings, *Nature* , *292*, 707–711.

Petit, J.-M., and M. Henon (1988), A numerical simulation of planetary rings. III - Mass segre-

gation, ring confinement, and gap formation, *Astron. Astrophys.,* , *199*, 343–356.

Salo, H. (1991), Numerical simulations of dense collisional systems, *Icarus*, *90*, 254–270.

Salo, H. (1992), Numerical simulations of dense collisional systems. II - Extended distribution of particle sizes, *Icarus*, *96*, 85–106.

Salo, H. (1995), Simulations of dense planetary rings. III. Self-gravitating identical particles., *Icarus*, *117*, 287–312.

Salo, H., J. Schmidt, and F. Spahn (2001), Viscous Overstability in Saturn's B Ring. I. Direct Simulations and Measurement of Transport Coefficients, *Icarus*, *153*, 295–315.

Schmit, U., and W. M. Tscharnuter (1995), A fluid dynamical treatment of the common action of self-gravitation, collisions, and rotation in Saturn's B-ring., *Icarus*, *115*, 304–319.

Showalter, M. R. (1991), Visual detection of 1981S13, Saturn's eighteenth satellite, and its role in the Encke gap, *Nature* , *351*, 709–713.

Showalter, M. R., J. N. Cuzzi, E. A. Marouf, and L. W. Esposito (1986), Satellite 'wakes' and the orbit of the Encke Gap moonlet, *Icarus*, *66*, 297–323.

Spahn, F., and H. Sponholz (1989), Existence of moonlets in Saturn's rings inferred from the optical depth profile, *Nature* , *339*, 607–608.

Spahn, F., and M. Sremčević (2000), Density patterns induced by small moonlets in Saturn's rings?, *Astron. Astrophys.,* , *358*, 368–372.

Spahn, F., and H.-J. Wiebicke (1989), Long-term gravitational influence of moonlets in planetary rings, *Icarus*, *77*, 124–134.

Sremčević, M., F. Spahn, and W. J. Duschl (2002), Density structures in perturbed thin cold discs, *Mon. Not. R. Astron. Soc.,* , *337*, 1139–1152.

Wisdom, J., and S. Tremaine (1988), Local simulations of planetary rings, *Astron. J.,* , *95*, 925–940.

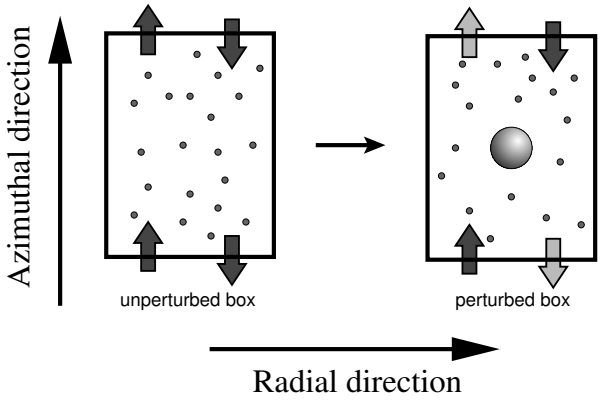


**Figure 1.** Ingredients of the moonlet simulation. The frame in the left depicts an unperturbed simulation region with periodic azimuthal boundaries. Particles leaving the region are introduced back from the opposite face (dark arrows). In the perturbed case the particles leaving the region are discarded (light arrow), and the phase space distribution of incoming particles is taken from the corresponding unperturbed simulation (same particle properties, optical depth).

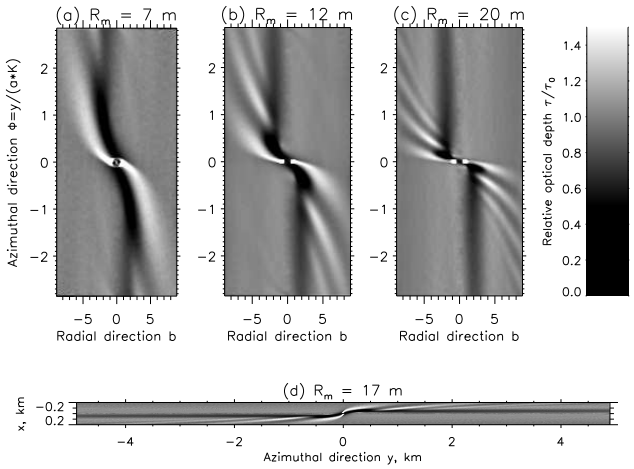


**Figure 2.** Steady-state density response for different sized moonlets. The plots are shown in scaled coordinates (a) $R_m$ = 7m, (b) $R_m$ = 12m and (c) $R_m$ = 20m. Part (d) shows the resulting density of a $R_m$ = 17m moonlet in physical units with a correct aspect ratio, i.e. how it might appear in Cassini imaging data.

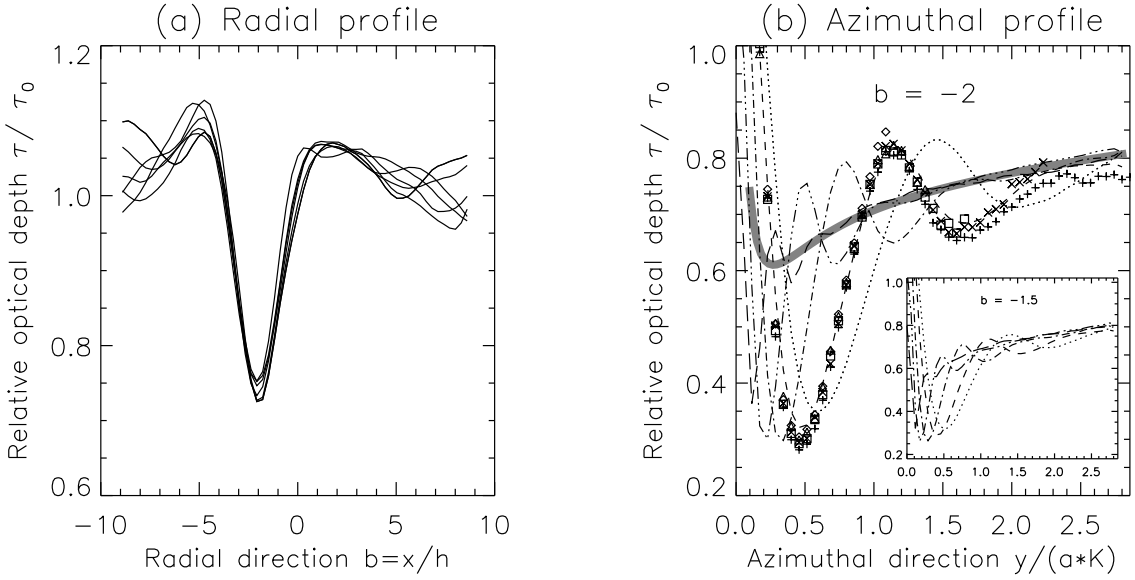


**Figure 3.** Radial and azimuthal profiles of the propeller. Part (a) shows the azimuthal averaged radial profile (for $\phi > 1$, excluding the vicinity of the moonlet) for moonlet radii $R_{\rm m}$ = 9 ...20 m. Part (b) shows the azimuthal profile at b = 2 scaled in $a_0 \cdot K$. Only the quadrant of the perturbed outgoing particles is presented ($b < 0$ and $\phi > 0$). The thick gray solid line represents the approximate analytical solution (*Sremčević et al.* [2002] , see their figure 10 (c)). The other lines are simulation data for different sized moonlets: (i) $\cdots$ $R_{\rm m}$ = 9 m, (ii) - - - $R_{\rm m}$ = 10 m, (iii) $-\cdot-$ $R_{\rm m}$ = 12 m, (iv) $-\cdots-$ $R_{\rm m}$ = 15 m and (v) $---$ $R_{\rm m}$ = 20 m. The symbols correspond to simulations of a $R_{\rm m}$ = 10 m moonlet, but with different azimuthal box size: $\diamond$ $L_y$ = 1.1 $a_0K$, $\triangle$ $L_y$ = 1.4 $a_0K$, $\square$ $L_y$ = 1.6 $a_0K$, $\times$ $L_y$ = 2.2 $a_0K$ and + $L_y$ = 5.4 $a_0K$. The inserted plot illustrates the azimuthal profile at $|b|$ = 1.5, where the wakes no longer appear and thus the scaling works much better.

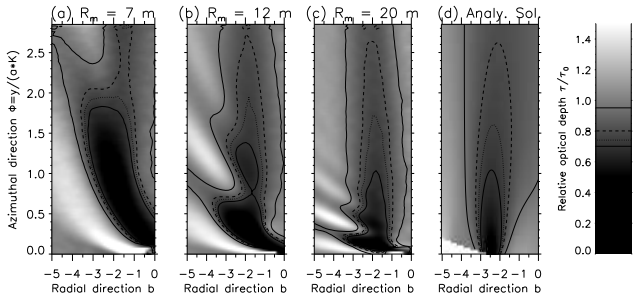


**Figure 4.** Gray-coded densities for different sized moonlets. Part (a) - (c) show the resulting density fields for the moonlets $R_{\rm m}$ = 7m, 12m, 20m, whereas (d) represents the analytical solution (*Sremčević et al.* [2002], see their figure 10 (c)). Contour levels of the same style represent the same optical depth level in all plots.